Available online at www.sciencedirect.com
ScienceDirect
Earth and Planetary Science Letters 248 (2006) 851–867
EPSL
www.elsevier.com/locate/epsl

Experimental quantification of the fractionation of Fe isotopes during metal segregation from a silicate melt

Mathieu Roskosz [a,b,*], Béatrice Luais [b], Heather C. Watson [a], Michael J. Toplis [b,c], Conel M.O'D. Alexander [d], Bjorn O. Mysen [a]

[a] Geophysical Laboratory, Carnegie Institution of Washington, 5251 Broad Branch Road, N.W., Washington, DC 20015, USA
[b] Centre de Recherches Pétrographiques et Géochimiques, CNRS UPR 2300, 15 rue Notre-Dame des Pauvres, BP 20, 54501 Vandoeuvre-lès-Nancy Cedex, France
[c] DTP, CNRS-UMR 5562, Observatoire Midi-Pyrénées, 14 avenue Edouard Belin, 31400 Toulouse, France
[d] Department of Terrestrial Magnetism, Carnegie Institution of Washington, 5241 Broad Branch Road, N.W., Washington, DC 20015, USA

Received 15 November 2005; received in revised form 8 June 2006; accepted 25 June 2006
Available online 28 July 2006
Editor: G.D. Price

Abstract

Fractionation of Fe isotopes between a silicate melt and metallic alloys has been quantified experimentally at 1500 °C. The effects of oxygen fugacity and run duration have been investigated to distinguish between kinetic and equilibrium fractionations. A new experimental setup is presented, in which metallic Fe is produced by reduction of oxidized iron from a silicate melt due to a change of redox conditions. This metallic Fe is physically removed from the silicate and sequestered as a (Pt,Fe) alloy. Bulk analyses of the silicate and metallic fractions using multi-collector ICP-MS methods are coupled with in situ analyses using an ion microprobe.

Experimental results indicate that significant isotopic fractionation of Fe occurs during metal segregation. During the early stages of the experiments, we find evidence for kinetic fractionation caused by faster diffusion of ^{54}Fe along concentration gradients in the alloy. This process leads to the formation of a metallic phase which is isotopically light compared to the residual silicate (metal–silicate fractionation up to −2.35‰/a.m.u.). The data are used to quantify the difference in diffusion coefficient of each isotope of iron, providing a means to predict Fe isotope fractionation during Fe diffusion in metallic alloys.

On the other hand, this state of affairs is transient in nature, and at superliquidus temperature, the systems rapidly reach a state of isotopic equilibrium in which the metal is isotopically heavier than the silicate melt by about +0.2±0.15‰/a.m.u. These results are consistent with the range of variation observed in natural samples. These kinetic and equilibrium data provide an experimental framework to understand the observed variability among igneous and meteoritic materials formed at high temperature, particularly for iron and pallasite meteorites.

Keywords: Iron isotopes; Diffusion; Silicate melts; Metallic alloys; Experimental petrology; Meteorites

1. Introduction

Recent advances in mass spectrometry make it possible to measure isotopic variations of transition metals

* Corresponding author. Geophysical Laboratory, Carnegie Institution of Washington, 5251 Broad Branch Road, N.W., Washington, DC 20015, USA. Tel.: +1 202 478 8968; fax: +1 202 478 8901.
E-mail address: m.roskosz@gl.ciw.edu (M. Roskosz).

0012-821X/$ - see front matter © 2006 Elsevier B.V. All rights reserved.
doi:10.1016/j.epsl.2006.06.037

(Cu, Fe, Zn, etc.) in materials of interest to the earth sciences. This development has given rise to several ground-breaking studies, concentrated primarily on the characterization of natural materials, including extraterrestrial, igneous, biogenic and abiogenic sedimentary rocks [e.g., 1–6]. In the case of Fe, these results have generated considerable interest because it has been inferred that the isotopic ratios of this element might be a tracer of microbial activity, a conclusion supported by experimental studies of biological systems [1,7]. However, measurements on materials which are clearly abiogenic in origin demonstrate that Fe isotopic variability also occurs, for example, during igneous processes at high temperature and high pressure [4,5,8–10].

Different classes of meteorites and planetary bodies have been shown to exhibit distinct Fe isotopic ratios [3–5,8,9]. Isotopic variability has also been demonstrated in single samples, such as between different silicate minerals in rocks from the Earth's mantle, and between taenite and kamacite in Fe meteorites [8–10]. These latter examples demonstrate that Fe isotope data represent a new and potentially powerful geochemical probe to constrain the processes of planet formation and differentiation over a wide variety of length scales. However, quantitative interpretation of the observed isotopic variations is currently hampered by a lack of experimental data and theoretical understanding of Fe isotope fractionation. In particular, the potential role of kinetic effects, the time-scales of re-equilibration, and the equilibrium fractionation factors between different phases are largely unconstrained, at both low and high temperature and pressure.

Previous work has concentrated on aqueous abiotic and biotic systems at low temperatures and pressures (typically less than 400 K and 1 bar pressure). Those results indicate that Fe isotope fractionation mainly occurs during redox reactions [6,11–13], possibly associated with electron transfer [14]. Evaporation experiments have also been performed at high-temperature in a vacuum, producing Fe isotope fractionation of up to 40‰ between the gas and the residual solid as a result of Rayleigh distillation [18]. These values are large, but have been observed in some exotic natural materials [19–21]. In addition, moderate Fe evaporation is proposed to account for isotopic variations between planetary bodies such as Mars, Vesta, the Earth and the Moon [8]. On the other hand, no experimental studies exist that quantify the degree of isotopic fractionation that can be produced in high-temperature magmatic systems, yet some preliminary studies indicated that kinetic effects could fractionate Fe isotopes at high temperature [22–24].

From a theoretical point of view, consideration of Fe-bearing complexes in different structural environments indicates that Fe coordination significantly affects the isotopic fractionation factors between different Fe-bearing species [15–17]. Such theoretical studies are generally restricted (with one notable exception in [16]) to simple Fe-bearing complexes such as solvated Fe^{2+} and Fe^{3+} because an exhaustive knowledge of the vibrational modes of the compounds of interest is required to calculate the relevant fractionation factors. Redox reactions and coordination changes also occur in silicate and metallic melts during magmatic processes. It is possible that the important differences in the local bonding environment of Fe, and the redox contrast between liquid, mineral and metallic phases can result in detectable and interpretable isotopic fractionation.

Iron is present in both metallic and oxidized forms in materials from the inner solar system (e.g., chondrites, Fe meteorites, Earth-like planetary bodies, etc.). Thus, experimental determination of the fractionation produced during metal segregation is essential to understand the observed isotopic variability of extraterrestrial materials. Furthermore, the Fe isotope fractionation induced by metal extraction may also give insights into the process of planetary core formation because Fe is by far the most abundant component of the metallic phases present in planetary cores and meteorites [8,9]. As a first step towards an experimental determination of high pressure and temperature processes capable of fractionating Fe isotopes, we present experimental results for metal segregation from a silicate melt as a systematic function of oxygen fugacity and run duration. Results are consistent with the range of variation observed in natural samples and provide an experimental framework to understand the observed variability among igneous and meteoritic materials formed at high temperature.

2. Experimental approach

Iron alloys readily with noble metals such as Pt [e.g., 25]. This tendency has been known for several decades and has generally been considered as a problem by experimental petrologists because it results in Fe loss to the Pt containers [e.g., 26,27]. At high temperature the extent of these losses depends on temperature, oxygen fugacity, initial composition, run duration, pressure, and the relative volumes of the sample and its container [28]. Losses may vary from almost none to almost complete loss [27–29]. As a consequence of the experimental problems posed by the formation of (Fe,Pt) alloys, this system has been studied carefully, and activity–composition relationships have been quantified [30,31].

This "problem" of iron loss to noble metal containers has been used here to sequester metallic Fe in a physically separable form from the residual silicate. To limit the number of variable parameters, we studied a single melt composition at fixed temperature (1500 °C) and pressure (1 bar). This temperature was chosen in order to study a crystal-free silicate melt over a wide range of oxygen fugacity. Experiments were carried out at ambient pressure because the oxygen fugacity can be carefully controlled. The starting material was a glass of anorthite–diopside eutectic composition, considered to be a good analog of the 'silicate Earth', to which Fe was added in oxidized form (Table 1). A single large batch of glass was synthesized from mixtures of reagent grade SiO_2, Al_2O_3, $CaCO_3$, $MgCO_3$ and Fe_2O_3 that had been first fired at relevant temperatures to dehydrate them (between 300 and 1000 °C). The starting material was then melted in air in a thin-walled Pt crucible at 1500 °C for 1 h and then finely crushed.

Two sets of experiments were carried out to study the effect of oxygen fugacity on the system, and the effect of experimental duration. In the first case, approximately 200 mg of sample was loaded into an open Pt-capsule (of about 1 g). Only the bottoms of these capsules were welded, while the top was pinched to allow gas exchange between the sample and the furnace atmosphere. We used this design to have a large amount of Pt relative to the Fe in the initial silicate melt ($Pt/Fe_{total} \sim 50$). As a consequence, at any oxygen fugacity, the equilibrium composition of the (Fe,Pt) alloy is never reached and a significant flux of iron diffusing toward and alloying with the Pt-container is preserved during the experimental run. Experiments were performed in vertical gas-mixing furnaces in which the oxygen fugacity was controlled using CO/CO_2 gas mixtures. Experiments were terminated by drop quenching the charges into liquid water. The oxygen fugacity was varied from $\log(fO_2) = -0.7$ (air) to $\log(fO_2) = -8$ (just above the Fe–wüstite solid buffer) in order to cover the large range of oxygen fugacity relevant to Earth sciences. Run durations were all 24 h. After the quench, capsules were opened and the silicate and metal fractions were mechanically separated.

Table 1
Starting composition of the silicate fraction determined by electron microprobe

	Starting composition
SiO_2	47.63 (20) [a]
CaO	21.29 (11) [a]
Al_2O_3	14.79 (11) [a]
FeO [b]	8.90 (21) [a]
MgO	6.57 (05) [a]

[a] Error on the two last digits.
[b] Added as Fe_2O_3.

Time series experiments were performed using the Pt wire loop method. In this case glass droplets of approximately 25 mg were prepared. All the wire loops had the same weight (about 13 mg) and shape, and the low Pt/Fe_{total} (~ 5) ratio allows the (Fe,Pt) alloy to reach its equilibrium composition. Moreover, this design is amenable to modeling composition and isotopic profiles since the platinum wire loop may be considered as a cylindrical body immersed in the silicate liquid. There is no gas–platinum interface and the diffusion is isotropic and proceeds radially. Comparatively, capsules are less amenable to modeling because of the complicated geometry of their tops and bottoms, the non-radial diffusion and the presence of gas–platinum interfaces. For each experimental condition, two samples were treated together. All the experiments were performed at $\log(fO_2) = -5$ and 1500 °C. After the quench, one of the pair of samples was analyzed by electron microprobe to quantify compositional gradients of Fe in the silicate glasses and Pt wires. The same section was then used to determine isotopic compositions by ion microprobe. The second experimental charge of each run was analyzed by MC-ICP-MS to quantify the change in isotopic compositions of bulk metal and bulk silicate reservoirs.

3. Analytical methods

For the time series experiments, bulk samples were digested in concentrated $HF + HNO_3$ at 50 °C, and the Pt-wire loops were subsequently removed from the vial. For fO_2 series experiments, the platinum capsule was mechanically separated from the silicate, and silicate fractions were dissolved in $HF + HNO_3$. The platinum fraction was leached with HF at 50 °C to remove any silicate contamination. These HF solutions were then added to the respective digested silicate fractions. Pt-fractions were then dissolved in aqua regia. A sample of the initial Pt wire used for these experiments was also dissolved and its Fe content measured by ICP-MS. No significant amount of Fe was detected in the starting wire, and thus the Pt reservoirs are considered to be Fe-free at time = 0. The leaching of Pt fractions with HF and $HF + HNO_3$ is very unlikely to produce any measurable fractionation as Pt and Pt-rich alloys cannot be dissolved by any acids but aqua regia at high temperature [32]. Moreover, the very low diffusion coefficient of Fe in Pt at ambient temperature makes any migration of iron through the Pt fraction unrealistically slow. Furthermore,

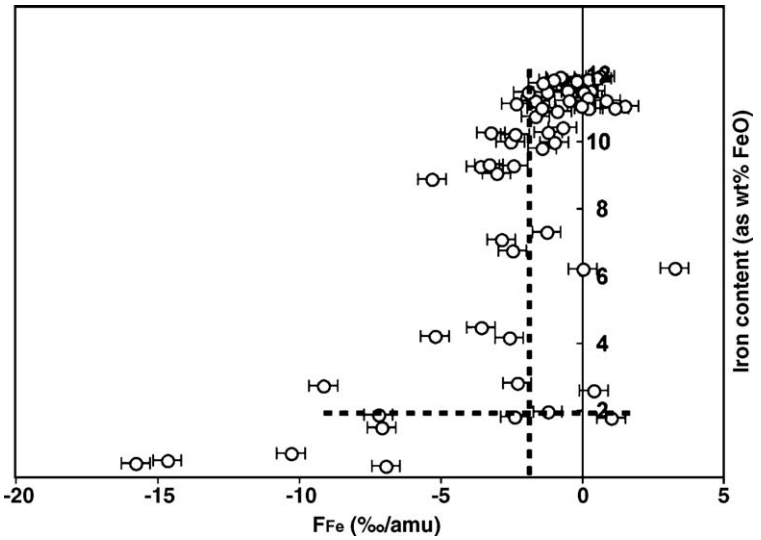

Fig. 1. Fe content vs. Fe isotopic ratio measured on Pt wires by ion microprobe. Dashed lines are guides for the eyes and highlight the absence of a strong correlation between Fe content and isotopic composition. This lack of direct correlation indicates that measured fractionation is not caused by matrix effects associated with variations in the composition of the (Fe,Pt) alloy, a conclusion also supported by mass-balance calculations, as demonstrated below.

if any iron were leached during this stage, only the very surface of the sample, which represents an insignificant fraction of the total iron alloyed with platinum, would be affected.

The digested metal and silicate fractions were dried down at 50 °C, dissolved in 6 M HCl for conversion to chlorides and to eliminate any residual fluorides, then dried down again. Samples were then re-dissolved in 7 M HCl, and loaded in 7 M HCl+0.001% H_2O_2 on AG-MP1 anion-exchange resin. H_2O_2 was added to prevent the conversion of Fe(III) to Fe(II) during column processing, these two species having distinct partition coefficients with respect to the resin. Matrices of the silicate fractions were first eluted with 7 M HCl+H_2O_2, while Pt from the Pt fractions remained absorbed on the anion resin at high HCl molarity. Fe was extracted in 2 M HCl+H_2O_2 [33]. Elution curves and concentrations determined by quadrupole ICP-MS indicate that yields are better than 99.6%, leading to undetectable isotopic fractionation during the entire separation procedure.

For the fO_2-controlled series, Fe isotopic measurements were performed on a multi-collector ICP-MS (MC-ICP-MS; Isoprobe GV Instruments, CRPG-Nancy) equipped with a hexapole collision cell. The machine was operated in a hard extraction mode, consisting in a 600 V potential applied to the collimator cone. Argide interferences on masses 54 (ArN), 56 (ArO) were rendered undetectable by using the Aridus desolvating nebuliser (without N_2 flow) and Ar+H_2 gases in the collision cell (for ArO and ArN), but argides at mass 57 (ArOH) remained non-negligible. These ArOH interferences are not formed by H_2 gas injection in the collision cell, as their level does not increase with increasing H_2

Table 2
Iron isotope results from fO_2 series experiments

Log (fO_2)	Fe fraction lost in Pt	$F_{Fe_{silicate}}$ (‰/a.m.u.)	Uncertainty (2σ)	$F_{Fe_{platinum}}$ (‰/a.m.u.)	Uncertainty (2σ)	$F_{Fe_{bulk}}$ [a] (‰/a.m.u.)	Uncertainty (2σ)	$F_{Fe_{M\text{-}S}}$ [a] (‰/a.m.u.)	Uncertainty (2σ)
−0.69	0.02 (1) [b]	0.057	0.048	−0.447	0.09	0.046	0.046	−0.504	0.102
−2.82	0.12 (2) [b]	0.23	0.05	−1.08	0.09	0.069	0.054	−1.311	0.103
−5	0.46 (1) [b]	1.042	0.042	−0.844	0.043	0.171	0.038	−1.886	0.061
−6	0.64 (3) [b]	1.292	0.024	−0.56	0.09	0.112	0.088	−1.852	0.093
−8	0.98 (1) [b]	2.407	0.033	0.064	0.09	0.108	0.09	−2.343	0.096

[a] Values calculated.
[b] Error on the last digit.

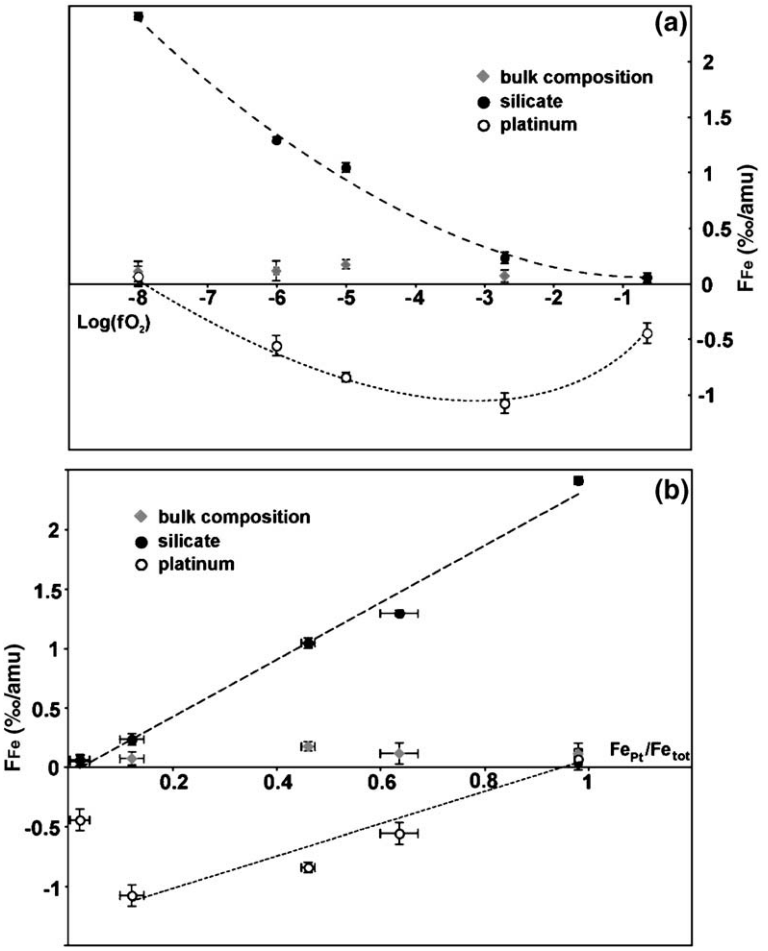

Fig. 2. Iron isotopic composition of silicate and metal fractions segregated as a function of (a) the oxygen fugacity and (b) the fraction of Fe lost from the silicate melt, at 1500 °C for 24 h. Measurements were carried out on the isoprobe (CRPG-Nancy, France). Bulk compositions are calculated from metal and silicate isotopic compositions and their relative abundance. Error bars are 2σ external reproducibility on $n=3$ replicates. Data are reported in Table 2. Dashed lines are only guides for the eyes.

flux. Typical Ar and H_2 flux in the hexapole collision cell of 1.2 and 1.6 ml/mn, respectively, and settings of the hexapole RF amplitude to 50% were adjusted for good compromise between maximum intensity of Fe and reduction of ArOH interferences. ArOH were further reduced to low levels by on-peak zero corrections. Because pure synthetic samples were used, ^{52}Cr (83.8%) was not detectable, and therefore, a Cr interference at mass 54 (2.3%) was not an issue. Analyses of 100–250 ppb diluted IRMM-014 Fe international standard give a beam intensity of about 15–20 V/ppm at ^{56}Fe. The time series experiments were analyzed on the MC-ICP-MS (Axiom, DTM Washington, DC). Isobaric interferences were removed using the 'cold plasma ICP-MS technique' described and validated elsewhere [5]. This technique relies on reduced temperature operation of the ICP source to eliminate molecular interferences from Ar complexes. Only masses 54 and 56 were measured because hydrides are formed in cold plasma, producing a ^{56}FeH interference at ^{57}Fe. On both instruments, instrumental mass bias was corrected using the standard-sample bracketing approach with respect to the same batch of IRMM-014 Fe isotopic standard, with concentration matching standard and sample to within 7%.

The isotopic ratios reported below are expressed as ‰/a.m.u.:

$$F_{\mathrm{Fe}} = \left(\frac{{}^{i}\mathrm{Fe}/{}^{j}\mathrm{Fe}_{sample}}{{}^{i}\mathrm{Fe}/{}^{j}\mathrm{Fe}_{standard}} - 1 \right) \bullet \frac{10^3}{i-j}$$

where ${}^{i}\mathrm{Fe}/{}^{j}\mathrm{Fe}_{\mathrm{sample}}$ is the measured ${}^{i}\mathrm{Fe}/{}^{i}\mathrm{Fe}$ ratio in the sample and ${}^{i}\mathrm{Fe}/{}^{j}\mathrm{Fe}_{\mathrm{IRMM\text{-}014}}$ is the average of the ${}^{i}\mathrm{Fe}/{}^{j}\mathrm{Fe}$ ratio of the standard (IRMM-014 for measurements

performed on MC-ICP-MS) measured before and after the sample in the analytical sequence. The external reproducibility, obtained through at least three replicate measurements, is better than 0.07‰/a.m.u. (2σ) on the Isoprobe and 0.1‰/a.m.u. (2σ) on the Axiom. For the Isoprobe, long-term (8 months) external reproducibility estimated from measurements of the geostandard IF-G, including chemistry and analyses, is better than 0.08‰/a.m.u. (2σ) (van Zuilen and Luais, personal communication).

In situ Fe isotope measurements were carried out with an Cameca 6f ion microprobe at the Carnegie Institution of Washington using a 12.5 kV O^- primary beam, a 10 kV secondary accelerating voltage, a 50 eV energy window and 400 μm field aperture. The details of the analytical procedure have been published elsewhere [21]. The chamber pressure during analysis was $\leq 10^{-9}$ Torr. A focused primary beam (1–3.5 nA) was rastered in dynamic transfer mode over an area of 20×20 μm. Because of potential interferences at other masses, only ^{56}Fe and ^{57}Fe were measured. Analyses were performed at a mass resolution of ~8000, enough to resolve ^{56}FeH from ^{57}Fe. The external reproducibility is better than 0.766‰/a.m.u. (2σ).

Because of hypothetical matrix effects, IRMM-014 could not be used as a standard. In place of this pure Fe standard, we used a Pt wire that had been equilibrated for 24 h with the silicate melt. The Fe content of the wire was homogenous (~11.5 wt.%) and its isotopic composition with respect to the IRMM-014 Fe isotopic standard ($F_{Fe} \sim 0$‰/a.m.u.) was determined using MC-ICP-MS. This standard was used to determine sensitivity factors and instrumental mass fractionation factors. In principle, this correction does not completely account for a possible matrix effect due to variations of the Fe content of the different alloys analyzed. However, it is the most accurate correction available. Furthermore, there is no obvious correlation between Fe-content and F_{Fe} determined on the different samples by the ion probe. For a Fe content of about 2 wt.%, F_{Fe} varies from 0 to −9‰/a.m.u. (i.e., almost the complete range of isotopic variations), and conversely, $F_{Fe} \sim -1$‰/a.m.u. is measured for alloys containing from 2 to 11.5 wt.% of Fe (Fig. 1). Finally, as detailed in Section 5.1, the isotopic and compositional gradients measured by ion and electron microprobes, respectively, were used to calculate the bulk Fe isotope compositions of each sample. As shown below, these estimates are in remarkable agreement with data collected by MC-ICP-MS on samples prepared under similar experimental conditions. In conclusion, matrix effects or any other analytical artifact cannot be the cause of the isotopic variations described below.

4. Results

4.1. Fe isotope fractionation as a function of oxygen fugacity

The fraction of Fe lost from the melt increases steadily as $\log(fO_2)$ decreases (Table 2). After 24 h the Fe loss to the Pt capsule from a melt in air is very limited (2% of the total). It reaches more than 98%, however, at an oxygen fugacity of 10^{-8} bar (Table 2). Under these conditions, isotopic fractionation varies dramatically (Fig. 2a, b; Table 2). Metal segregation leads to the formation of an alloy in which the Fe is isotopically lighter than the starting glass, whereas the residual Fe in the silicate melt is isotopically heavier than the starting glass. With decreasing oxygen fugacity, the silicate residues become increasingly isotopically heavy, such that at $\log(fO_2) = -8$ the F_{Fe} of the silicate melt reaches 2.4‰/a.m.u. compared to the starting materials. To a first approximation, the isotopic composition of the silicates is a linear function of $\log(fO_2)$, although the sample produced in air does not lie on the trend defined by the other data (Fig. 2a). This non-linearity mirrors that observed for the proportion of Fe lost to the alloy (Table 2). As a consequence, the observed isotopic fractionation in the residue can be readily described as a linear function of the proportion of Fe lost to the alloy (Fig. 2b).

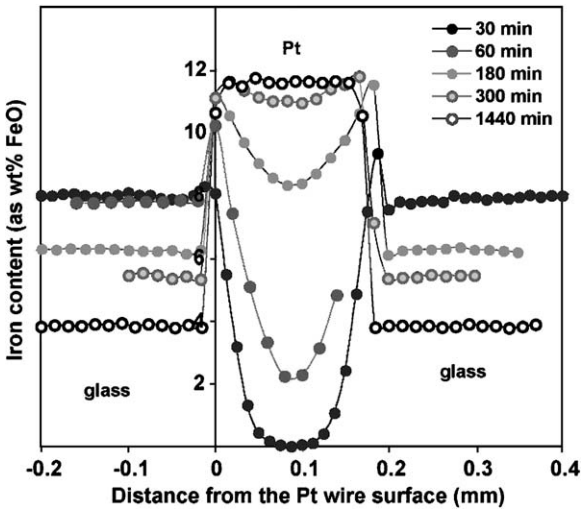

Fig. 3. Iron content of Pt wires equilibrated at $\log(fO_2) = -5$ for different durations. Error bars are typically the same size as symbols. Determination of Fe content near the metal–silicate interface may be inaccurate for short duration experiments due to missed local Fe enrichment of the Pt wire at the interface. This effect is illustrated by the asymmetrical shape of the profile performed on the sample heated for 30 min.

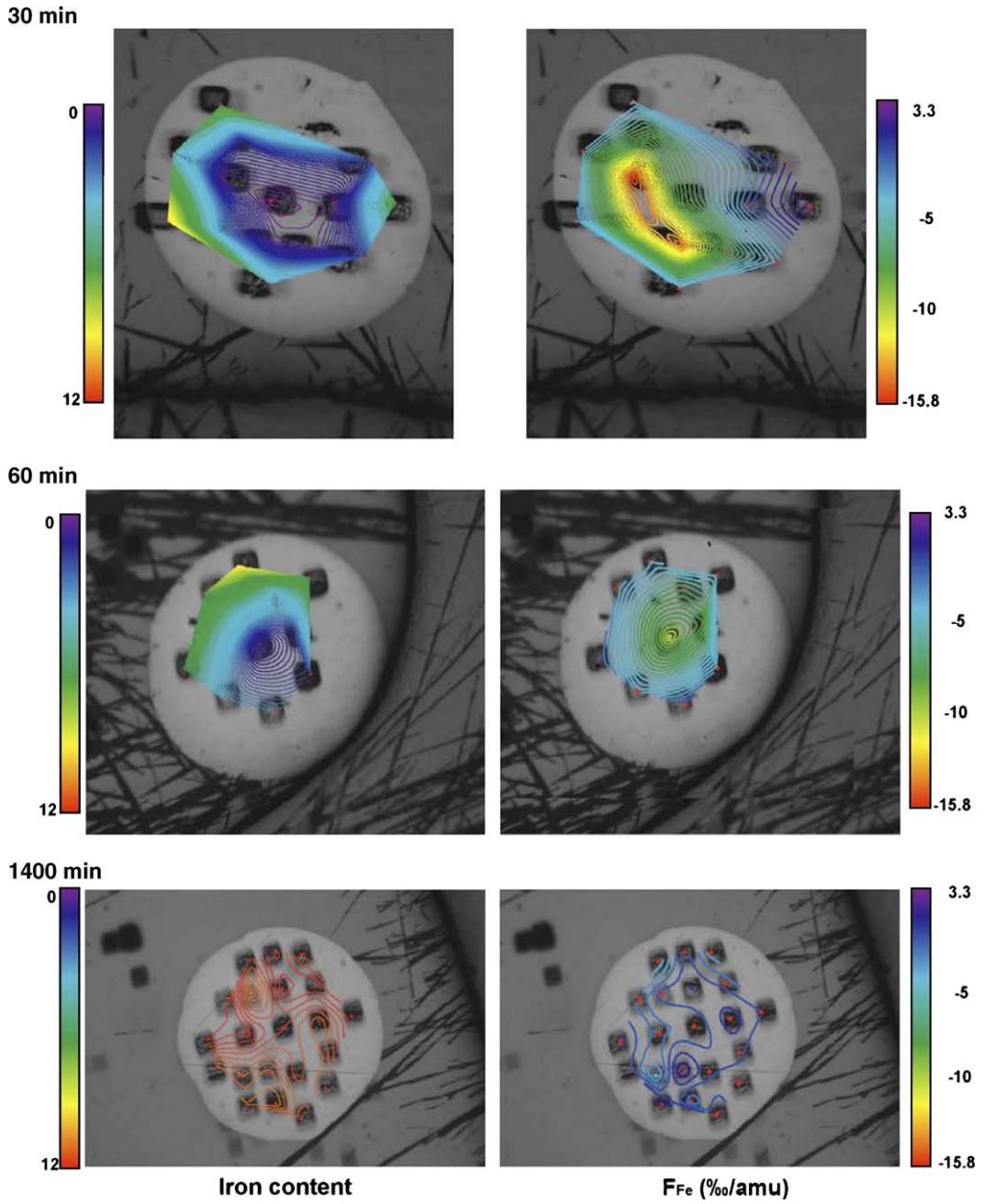

Fig. 4. Iron contents and isotopic compositions determined by ion microprobe on samples equilibrated for several durations. Only platinum wires were analyzed (see Analytical methods). All the Pt wires are 200 μm in diameter and are imaged here as light grey disks, surrounded by the silicate glass. Analyzed spots are seen as dark grey sputtering craters. Contour lines represent variations of 0.5% and 0.5‰/a.m.u., respectively. With increasing time, compositional and isotopic gradients disappear.

The isotopic composition of the (Fe,Pt) alloy shows a more complicated variation as a function of oxygen fugacity (Fig. 2a, b). The Fe in the alloy produced in air has a F_{Fe} of −0.45‰/a.m.u., the one produced in pure CO_2 atmosphere ($\log(fO_2)=-2.82$) is lighter with a F_{Fe} of −1.05‰/a.m.u. At still lower fO_2, F_{Fe} become less negative, reaching a value close to zero at $\log(fO_2)=-8$ (comparable to that of the starting material as demonstrated below by mass balance calculations).

The isotopic compositions of the bulk samples (i.e., melt+alloy) at each fO_2 have been calculated using the F_{Fe} values and Fe concentrations of each reservoir. No

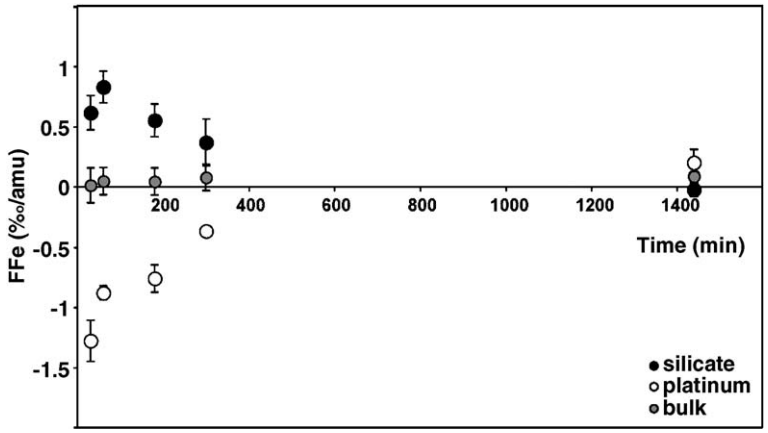

Fig. 5. Isotopic compositions of silicate and metal fractions segregated at 1500 °C, $\log(fO_2)=-5$ and different run durations. Bulk compositions represent calculated compositions as in Fig. 2. Errors bars are 2σ external reproducibility on $n=3$ replicates. Data are reported in Table 3.

significant deviation from one sample to another is observed within error (Fig. 2a). The system is thus closed from an isotopic perspective and evaporation is not responsible for the isotope fractionations revealed here.

If a single high-temperature process were at work, the isotopic composition of the silicate and the metal should be monotonic and co-linear functions of the fO_2. The more complicated trends actually observed indicate that the measured fractionations are the result of a kinetic fractionation process during the formation of the alloy. In this case, values do not necessarily represent a state of equilibrium, and re-equilibration may occur. As a consequence, the time dependence of the fractionation has been considered in more detail.

4.2. Isotopic fractionation of Fe as a function of time

As mentioned above, the experimental design used for the time-series experiments employed wire loops such that the bulk Pt/Fe_{total} was low. Typical elemental diffusion profiles are observed within the Pt wire whereas the Fe contents of silicate glasses are homogeneous for a given experimental charge (Fig. 3). Diffusion of Fe in the melt is thus significantly faster than in Pt. This latter effect controls the overall rate of metal–silicate equilibration. More than 8 h are typically required to reach equilibrium concentrations of Fe throughout the alloy at 1500 °C (see below).

Ion probe measurements indicate that Fe isotopes are strongly fractionated along concentration gradients (Fig. 4). For the shortest duration run (30 min), the fractionation between the center and the surface of a Pt wire reaches $F_{Fe}=14$‰/a.m.u., the Fe in the center of the charge being isotopically lighter than the Fe dissolved in the outer part of the wire.

Bulk MC-ICP-MS analyses indicate that the isotopic compositions of metal and silicate reservoirs change as a function of time (Fig. 5 and Table 3). However, the computed bulk compositions of the systems (alloy+silicate) do not. This indicates again that no evaporation of Fe occurred during the experiments or that if it did, no significant isotopic effects were induced. For experiments shorter than 5 h, results are consistent with the data previously described. High-temperature segregation of Fe

Table 3
Iron isotope results from time series experiments

Run duration (min)	$F_{Fe_{silicate}}$ (‰/a.m.u.)	Uncertainty (2σ)	$F_{Fe_{platinum}}$ (‰/a.m.u.)	Uncertainty (2σ)	$F_{Fe_{bulk}}$ (‰/a.m.u.)[a]	Uncertainty (2σ)	$F_{Fe_{M\text{-}S}}$[a] (‰/a.m.u.)	Uncertainty (2σ)
30	0.665	0.143	−1.228	0.17	0.004	0.174	−1.893	0.223
60	0.879	0.131	−0.829	0.059	0.04	0.112	−1.707	0.144
180	0.601	0.136	−0.709	0.114	0.036	0.113	−1.311	0.178
300	0.418	0.194	−0.315	0.028	0.07	0.109	−0.733	0.196
1440	0.025	0.107	0.249	0.111	0.114	0.078	0.224	0.154

[a] Values calculated.

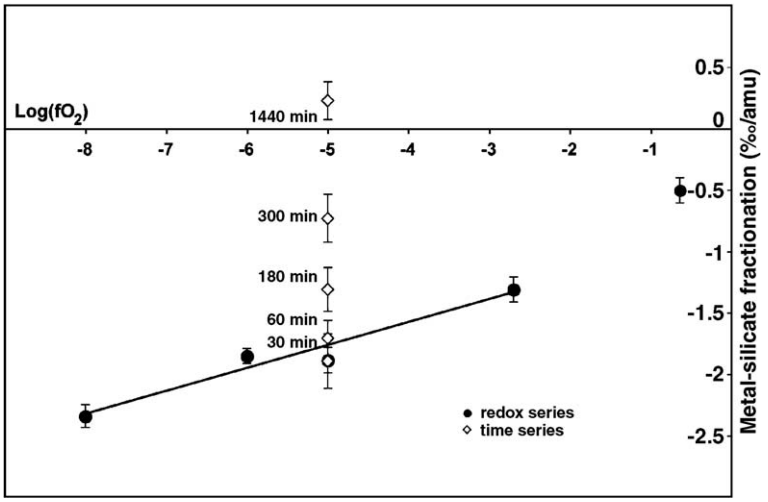

Fig. 6. Metal–silicate fractionation of iron isotopes as a function of oxygen fugacity and in the absence of alloy Fe-saturation (black dots). Metal–silicate fractionation as a function of time with possibility of saturation and re-equilibration (open diamonds).

from a silicate initially leads to an alloy with a light isotopic composition (F_{Fe}=−1.3‰/a.m.u.), the residual silicate being heavier than the initial material (F_{Fe} up to 0.85‰/a.m.u.). However, the difference in isotopic composition between reservoirs decreases with time, even crossing zero, such that in the longest duration experiments, F_{Fe} of the silicate fraction is slightly lighter than that of the alloy.

Several lines of evidence suggest that the time-dependent fractionation of Fe isotopes is primarily diffusion-controlled. The clearest evidence is obtained from the isotopic profiles, which are found to occur along concentration gradients of Fe. Detailed and quantitative consideration of these data is provided below. We also note that the bulk isotopic compositions measured by MC-ICP-MS are consistent with a diffusion process.

4.3. Comparison between fO_2 and time series experiments

The time series demonstrate that isotopic re-equilibration of the alloy and the silicate occurs. This point is clearly illustrated by the combination of the two different sets of experiments (Figs. 2 and 5). For instance, at log (fO_2)=−5, T=1500 °C and t=24 h, the isotopic composition of the (Pt,Fe) capsule is about −0.85‰/a.m.u., whereas that of the (Pt,Fe) wire loop is ~0.2‰/a.m.u. This difference is the result of the different experimental designs employed. In the experiments with high Pt/Fe_{total}, the equilibrium composition of the (Fe,Pt) alloy is far from being reached even after 24 h. Conversely, the equilibrium composition of the alloy is rapidly reached in the time series experiments, performed on samples having a low Pt/Fe_{total}.

These two different setups are thus complementary and self-consistent as demonstrated when the inter-reservoir fractionation is plotted as a function of fO_2 and run duration (Fig. 6). The fO_2 series provide an example of the extreme fractionations that can be measured between silicate and metal reservoirs during a unidirectional diffusion process. This fractionation is controlled by the same driving force as that leading to diffusion. In this respect, the strong dependence as a function of oxygen fugacity (Fig. 2) is the consequence of the increase of Fe activity in (Fe,Pt) alloys under increasingly reducing conditions [28]. Because of that, the driving force for diffusion increases when fO_2 decreases because the Fe content of the (Fe,Pt) alloy at equilibrium increases dramatically.

Turning to the time series data, samples treated at log (fO_2)=−5 for short run durations (less than an hour) exhibit the same inter-reservoir isotopic fractionation as in fO_2 experiments, which indicates that at both experimental conditions (i.e., different Fe/Pt ratios and different time durations but same fO_2 and T), the driving force was similar. For longer run durations, isotopic ratios tend toward less extreme values (Figs. 5 and 6). This re-equilibration of both reservoirs is probably made possible by the gradual decrease of the difference between the Fe content of the alloy at a given time and the Fe content of the alloy at equilibrium. Qualitatively, this provides an explanation for the observation that the isotopic composition of the alloy is a non-linear function of log(fO_2). In air, the solubility of Fe in Pt is very low, and thus, the driving force for the diffusion of Fe into Pt

is low. In this case, re-equilibration between the alloy and the silicate is almost complete after 24 h.

5. Discussion

5.1. Diffusion-controlled fractionation of Fe isotopes

Formation of the alloy is clearly a multi-stage process involving several steps, from the reduction of Fe oxides in the silicate melt to the diffusion of Fe into Pt to reach the equilibrium composition of the alloy at given T and fO_2.

It is not clear whether processes taking place in the liquid or at the metal–silicate interface may potentially affect isotopic fractionation. However, reduction of the melt occurs on short time-scales relative to the experimental durations [34]. Therefore, if the processes taking place in the melt result in isotopic fractionation, a rapid re-equilibration between different species should also occur. Furthermore, ion microprobe data indicate that the isotopic composition at the surfaces of the Pt wire is constant over time (Fig. 7) and electron microprobe data show that the surface of Pt wires are saturated in Fe very shortly after the change of redox conditions (Fig. 3). It is thus unlikely that processes taking place at the metal–silicate interface explain the large fractionations observed.

The most likely origin for the kinetic fractionation of Fe during alloy formation is the diffusion of Fe into the alloy. An accurate description of diffusion processes in the alloy is thus required. The diffusion coefficient of Fe in Pt at 1500 °C can be extracted from the observed profiles (30, 60, 180, 300 min) by fitting them with the equation for diffusion into a cylinder from a stirred solution of limited volume with constant diffusion coefficient [35]. In this case, the ratio of the total mass uptake (M_T) at a given time to the equilibrium value (M_∞) can be used. The solution is:

$$\frac{M_T}{M_\infty} = 1 - \sum_{n=1}^{\infty} \frac{4\alpha(1+\alpha)}{4 + 4\alpha + \alpha^2 q_n^2} e^{-Dq_n^2 t/a^2} \quad (1)$$

where D is the diffusion coefficient, a is the radius of the wire, $\alpha = A/\pi a^2 K$ or the ratio of the volumes of the melt and the cylinder, including the effect of the partition coefficient, K, (A being the area of the melt, excluding the wire). K was taken as 2.965, which is the ratio of Fe contents in the wire and the melt at equilibrium. The q_ns are the positive, non-zero roots of the equation:

$$\alpha q_n J_0(q_n) + 2J_1(q_n) = 0, \quad (2)$$

where the J's are Bessel functions of zeroth and first order, respectively. The ratio of the mass uptake was

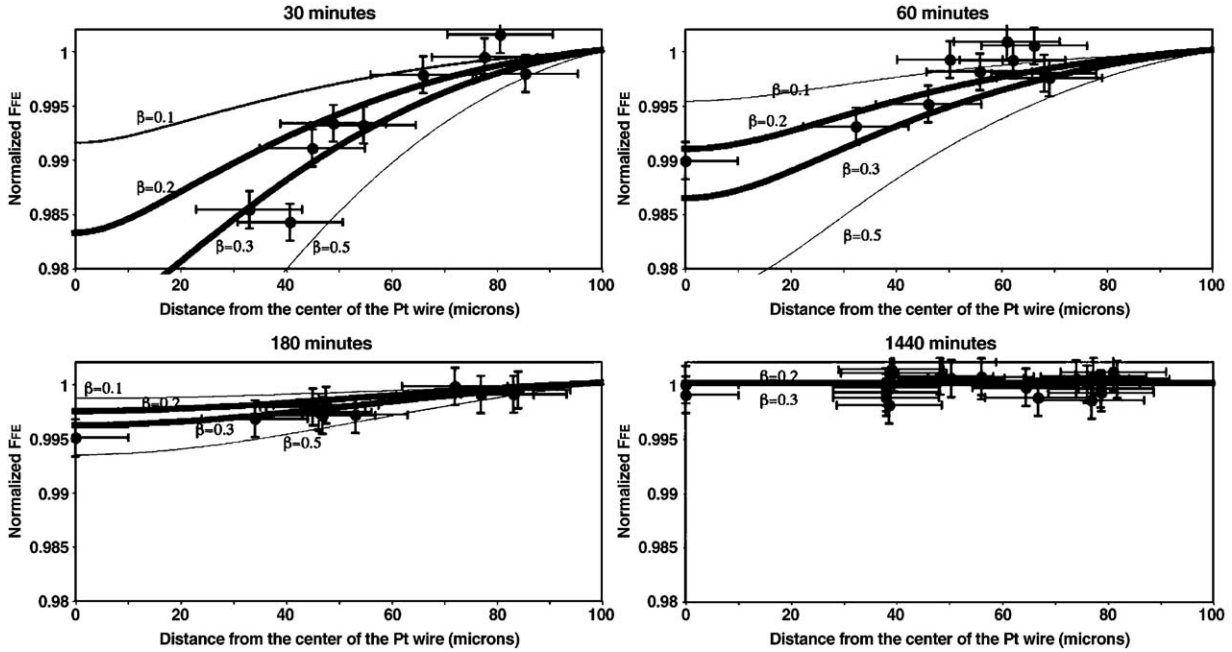

Fig. 7. Experimental and calculated isotopic profiles determined by ion microprobe on Pt wires as a function of time. Samples and data are those mapped in Fig. 4. Empirical Eq. (4) has been used to calculate profiles (see text for methods). The value of parameter β is between 0.2 and 0.3 (best value 0.27). Data are normalized to the average ratio determined on the sample equilibrated for 24 h (see Analytical methods).

determined for each experiment by integrating under the measured concentration profile in the wire (M_T). This value was divided by the equilibrium value (M_∞).

The right hand side of the equation was solved for the first 100 terms of the sum, which converges rapidly. A plot of M_T/M_∞ vs. $\sqrt{(Dt/a^2)}$ gives D, as a^2 and t are known quantities. D is taken to be 2.6×10^{-13} m^2 s^{-1}, which is the average value calculated for the four experiments. The slightly lower values for D in the shorter duration experiments are likely due to a high concentration of Fe near the melt/wire interface that was missed in the electron microprobe analyses because of the relatively wide spacing between analysis points (Fig. 3), which further results in a lower calculated M_T, and thus, a lower diffusivity. Based on these calculations, the hypothetical equilibrium is reached after 530 min.

In light of the constraints provided by this analysis, we will now consider the elemental and isotopic variations as a function of distance in the alloy. In this case, the concentration profile can be calculated for the case of diffusion into a cylinder from the following equation [35]:

$$C_{r,t} = C_\infty \left\{ 1 + \sum_{n=1}^{\infty} \frac{4(\alpha+1)e^{-Dq_n^2 t/a^2}}{(4+4\alpha+\alpha^2 q_n^2)} \frac{J_0(q_n r/a)}{J_0(q_n)} \right\}. \quad (3)$$

Using the calculated value for D (2.6×10^{-13} m^2 s^{-1}) in this equation and calculating the sum for the first 100 terms reproduce the experimental data satisfactorily (Fig. 8). The measured diffusivity for Fe in Pt is quite similar to previously measured values of Pt diffusion in Fe and Fe–Ni alloys. For instance, extrapolation of the data to 1500 °C predicts D_{Pt} in Fe to be 4.6×10^{-13} m^2 s^{-1} [36]. 1 GPa experiments at 1400 °C give D_{Pt} between 5×10^{-14} m^2 s^{-1} and 10^{-14} m^2 s^{-1} in Fe and $Fe_{90}Ni_{10}$, respectively [36,37]. The lower value of D in these latter experiments is consistent with lower temperature and slight negative pressure effect [37,38].

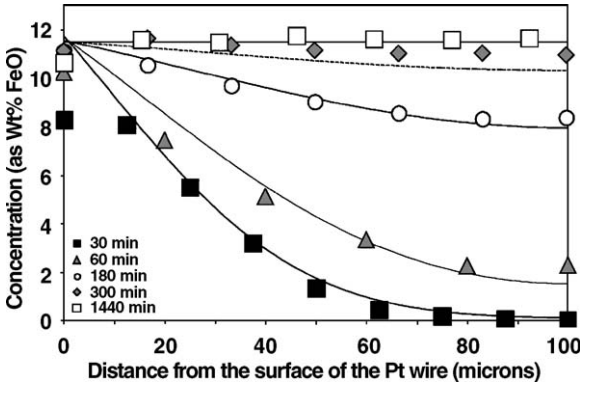

Fig. 8. Comparison between experimental data and diffusion profiles in Pt wires recalculated with $D=2.6\times10^{-13}$m^2 s^{-1} (see text for methods and error source analyses).

Table 4
Comparison between bulk F_{Fe} of Pt wires calculated from ion probe data and measured with MC-ICP-MS

Run duration (min)	$F_{Fe_{platinum}}$ ion probe (‰/a.m.u.)[a]	$F_{Fe_{platinum}}$ ICP-MS (‰/a.m.u.)
30	−1.473	−1.477
60	−0.957	−1.078
180	−1.255	−0.958
300	–	−0.564
1440	0	0

Data are given relative to the sample equilibrated for 24 h to insure consistency between both techniques. Typical uncertainties are 0.766‰/a.m.u. on ion probe data and 0.1‰/a.m.u. on ICP-MS data.
[a] Calculated by integrating isotopes gradients measured by ion probe (Fig. 7) and elemental gradients determined by electron microprobe (Fig. 8).

Turning now to isotopic fractionation, the ratio of diffusivities of different isotopes has been shown to follow an equation of the form:

$$D_1/D_2 = (m_2/m_1)^\beta, \quad (4)$$

where β is an empirical factor, and the D's and m's are the diffusivities and masses of the isotopes 1 and 2, respectively [39,40]. From the known diffusivity of Fe in Pt, we can then use this equation to model the measured profiles of the isotopic ratio. The value for D of 2.6×10^{-13} m^2 s^{-1} was thus assumed for ^{56}Fe (which is by far the most abundant isotope of Fe), and values of D ^{57}Fe were calculated assuming different values of β, ranging from 0.05 to 0.5. The best fit to the data obtained was for $\beta\sim0.27$. To solve for concentration profiles from Eq. (4) above, the first 100 terms of the sum were calculated for both ^{56}Fe and ^{57}Fe using their respective diffusivities for r=0–100 μm at 1 μm intervals (Fig. 7). The internal consistency between ion probe data and MC-ICP-MS data has been confirmed by the integration of these isotopic gradients. Mass-balance calculations were carried out by integrating both elemental gradients determined by electron microprobe (Fig. 8) and isotopic gradients determined by ion microprobe (Fig. 7). Within the uncertainties associated with the ion probe and ICP-MS data, the agreement is excellent (Table 4). This result demonstrates that ion probe data are not significantly affected by analytical artifacts. Thus, profiles analyzed here and the value of β derived from them are reliable.

Despite the fact that β is empirical and must be determined experimentally, kinetic theory applied to a perfect gas provides an upper limit of 0.5 for this parameter. For condensed matter, it is thus expected that β should be between 0 and 0.5. There are as yet very few studies of diffusion-driven isotopic fractionation. The experimental studies by Richter et al. [39,40], concerning liquid silicates provide the two most accurate determinations of β, which are 0.075 for $^{44}Ca/^{40}Ca$ and 0.215 for $^{7}Li/^{6}Li$. Another value (0.0969), determined by molecular dynamics calculation, has been proposed to account for the fractionation of Mg isotopes driven by diffusion in liquid MgO [41]. To our knowledge, no data are available for Fe-bearing metallic alloys. However, diffusion and isotopic data reported in [42] concern the diffusion of Ge in pure Cu. Applying Eq. (4), these data may be used to calculate β, which has a value of ~ 0.25. Despite the different diffusing species, metal matrix and temperature of study (860 °C vs. 1500 °C), the similarity of this value to that measured here for the diffusion of Fe in Pt is striking, and it is tempting to speculate that 0.25 is a typical value of β in metallic alloys in general. Indeed, this conclusion would appear to be supported by recent data on Tl isotope fractionation measured in sulfides nodules of iron meteorites [43]. As detailed below, those data point to diffusion-driven fractionation of Tl isotopes and a value in the range 0.15–0.3 is derived for β , perfectly consistent with the other available data for diffusion in metallic alloys.

Part of the problem is that there is no general understanding of how β varies as a function of the element of interest, the structural environment of that element, or the nature of its matrix. Based on the few published data and our experimental determination, we propose that the weaker the bonds between the element and the matrix, the higher the β parameter. This proposal satisfies the upper value of 0.5 for perfect gases. It is also consistent with the fact that lithium, which has a high β value, is known to interact very weakly with other cations in silicate melts. The opposite is true for calcium, which is a relatively strong network-modifying and charge-compensating cation. Within this framework, our relatively high value of β is simply interpreted as a reflection of the weak bonds characterizing the Fe environment in metallic alloys compared to the ionic-covalent bonds characterizing oxide systems. This description may also explain why, to a first approximation, a single value of β can be used to model the behavior of different elements in different alloys. More work is clearly needed but if confirmed, this result indicates that the behavior of Ni, Ge, or even W during differentiation processes may be easily amenable to modeling and that hypothetical contributions of diffusion-driven isotopes fractionations may be assessed.

5.2. Equilibrium fractionation between metal and silicate at high temperature

Equilibrium isotope fractionation is the result of differences in the zero point energy of molecules with different isotopic compositions [44]. It is a purely quantum effect in origin, which depends on the vibrational density of states of the materials studied. Even for solids, calculation of the vibrational density of states is very complicated. In the case of liquids, the situation is even worse because it is currently impossible to calculate the effect of isotopic substitution on configurational degrees of freedom. Even rough estimates using molecular dynamics are not yet available. Therefore, only experimental approaches can be used to determine the magnitude of the equilibrium isotope fractionation expected between a silicate melt and a metallic alloy.

Our time series experiments are a first step to constrain the equilibrium fractionation factor. As discussed above, elemental equilibration between the melt and the alloy is complete after 8–9 h. Interestingly, linear extrapolations of trends defined by the two reservoirs indicate that their isotopic compositions are the same within error after this duration (Fig. 5). But, further changes occur after 8–9 h that could indicate a gradual change toward a measurable equilibrium fractionation between a metal and a silicate melt. At 1500 °C and $\log(fO_2) = -5$, the measured isotopic difference between the metal and the silicate is 0.2 ± 0.15‰/a.m.u. At such a high temperature, if a measurable fractionation occurs it must be relatively small. Therefore, we consider 0.2‰ as an uppermost limit.

Though not directly comparable we can discuss this value in the light of theoretical studies which only deal with crystalline solids [15,16]. Under the conditions studied here, the experimentally determined fractionation is significantly higher than estimates from theoretical studies [15,16]. For example, using the reduced partition function ratio calculated for pure Fe metal and olivine crystals, the equilibrium fractionation at 1500 °C should be about 0.02‰/a.m.u. Our data are nonetheless consistent in that they indicate the formation of an isotopically heavy metal and a light silicate. However, the lowest value is still about three times higher than the rough theoretical prediction.

Several arguments may be invoked to explain this difference. First of all, calculation of the vibrational density of states may only be approximated for solids and a discrepancy by a factor of 3 may be considered reasonably good. Also, compositional differences may have a

significant effect. Indeed, the fractionation measured here is not between pure Fe metal and olivine, but between a liquid of anorthite–diopside eutectic composition and a (Fe,Pt) alloy. Finally, the structures, Fe coordination and density functions of olivine and silicate melt are significantly different. In this respect, structural differences between the silicate liquid and (Pt,Fe) alloy are larger than those existing between two ideal crystalline solids (Fe-metal and olivine). However, it is also worth noting that more extensive measurements must be carried out to confirm these preliminary data. In particular, reversal experiments using a (Fe,Pt) alloy and a Fe-free silicate melt as starting materials would provide more complete constraints on the equilibrium value of metal–silicate isotopic fractionation.

Finally, before discussing the implications of our results for natural systems, we must consider to what extent (Fe,Pt) alloys reflect the properties of (Fe,Ni) alloys in the context of metal/silicate segregation in geological systems. At temperatures higher than 1400 °C the system Fe–Pt shows complete solid solution. The high-temperature structure of an $Fe_{0.17}Pt_{0.83}$ alloy (the approximate composition of the alloys formed during our experiments) is similar to that of copper. It is a face-centered cubic structure (fcc) with a cell parameter of 3.888 Å [45]. Its structure is relatively disordered, Fe and Pt atoms are randomly distributed, and the coordination number of Fe is 12. The molar volume of the alloy shows a slight deviation from ideality, so it is possible that the molar volume of Fe in these alloys is slightly higher than that for pure Fe [29], but this difference is relatively small.

Iron–nickel alloys also form a complete solid solution at high temperature. Their structure is also fcc, similar to Cu, and the coordination number of Fe is again 12 [e.g., 46]. There are thus strong similarities between (Fe,Ni) and (Pt,Fe) alloys at high temperature. The only significant difference between the alloys studied here and natural (Fe, Ni) alloys is the Fe content. Here, it never exceeds 12 wt. %, while in natural alloys, the Fe content is rarely less than 90 wt.%. This compositional difference obviously has some consequences for the activity of Fe in the alloy that could in turn affect the equilibrium isotope fractionation. Nevertheless, these data provide a reasonable first approximation for the metal–silicate equilibrium fractionation in light of the strong structural similarity between (Fe,Pt) and (Fe,Ni) alloys.

5.3. Geochemical implications

The subject of Fe isotope geochemistry/cosmochemistry is a rapidly expanding field. In this respect, recent MC-ICP-MS studies have highlighted significant mass-dependent Fe isotope variations between metal and metal–silicate phases in iron meteorites and pallasites [3–5,9].

5.3.1. A diffusion-driven Fe isotopes fractionation recorded in iron meteorites?

Iron meteorites form a heterogeneous class of meteorites with very different compositions, trace element patterns, and microstructures [e.g., 47]. Despite this variability, the main iron groups are interpreted as being derived from the cores of separate differentiated asteroids [48]. As a consequence, their properties have been extensively studied because of their potential application to Earth-like planetary cores. The Widmanstätten pattern is one of the most studied properties of these meteorites because it can provide information on the cooling rates of the parent bodies [e.g., 49–55]. This pattern is a two-phase intergrowth of kamacite (α-bcc, Ni-poor phase) and taenite (γ-fcc, Ni-rich phase). The Widmanstätten texture forms by nucleation and growth of kamacite parallel to the octahedral plane (111) of taenite during slow cooling of the parent body [56]. This conventional interpretation, based solely on the binary Fe–Ni equilibrium phase diagram, is a first-order description of nucleation and growth processes in this system. Nevertheless, the major chemical and structural properties of the main groups of iron meteorites are defined by the subsolidus exsolution of kamacite from taenite.

Diffusion produced concentration profiles of Ni and trace elements like Pt, Pd, Au, Cu, Mo and Ge in kamacite laths may also be used to derive cooling rates of the parent meteorite bodies [e.g., 57,58]. While estimated cooling rates are still controversial within some groups of the iron meteorites (e.g., IVA) and may span several orders of magnitude [51,59,60], the presence of concentration gradients demonstrate that compositional equilibrium between taenite and kamacite is rarely achieved. Thus, the chemical features of these phases have to be interpreted within the framework of kinetic rather than equilibrium models.

A recent study of Fe isotope variability among kamacite and taenite laths indicates that Fe tends to be heavier in taenite compared to kamacite. Measured F_{Fe} is as high as 0.1/a.m.u. in the first phase and varies between 0.022‰/a.m.u. and 0.055‰/a.m.u. in the second [9]. These variations were interpreted to reflect the effect of the coordination number of Fe in these two phases (12 in taenite against 8 in kamacite) [9]. However, the measured fractionation is significant and appears to vary from one sample to another. For these reasons, a simple coordination change from 12 to 8 may not be enough to explain the data. On the other hand, our

results demonstrate that solid-state diffusion of Fe in an alloy is capable of producing a large fractionation of Fe isotopes. During this process, it is demonstrated that the initial reservoir becomes heavier whereas the newly formed alloy is significantly lighter than the source. The fractionation between kamacite and taenite may be explained in the same way, due to the diffusion controlled subsolidus exsolution of kamacite from taenite, followed by partial re-equilibration during cooling of the parent body. This interpretation is consistent with the characteristic time-scale for isotopic re-equilibration calculated by extrapolation of our data to lower temperature. Assuming that the diffusion coefficient of Fe in Pt shows Arrhenian behaviour and that the activation energy has a value of 308 kJ/mol, as shown to be the case for diffusion coefficients of other siderophile elements, in particular the diffusion of Re in Fe [61], we calculate diffusion coefficients of Fe in Pt of 7.1×10^{-17} m^2 s^{-1} and 3.1×10^{-19} m^2 s^{-1} at 1000 °C and 800 °C, respectively. In this case the time required to equilibrate two isotopic reservoirs across 200 μm with diffusion from both sides is on the order of ~5.4 yr at 1000 °C, ~1225 yr at 800 °C and ~2.25 my at 600 °C. Bearing in mind that final subsolidus formation of iron meteorites is inferred to occur through to even lower temperatures (700 °C to 400 °C), it is more than likely that a large fraction of iron meteorites is not completely equilibrated from the isotopic point of view. This conclusion is also consistent with recent isotopic data on Tl isotopes showing that diffusion-driven fractionation of Tl isotopes was significant in some iron meteorites [43].

A direct consequence is that Fe isotope fractionation may be used to quantify the degree of disequilibrium existing between the two phases. Provided that laser-ablation ICP-MS or ion probe techniques are capable of measuring Fe isotope ratios along taenite–kamacite intergrowths, our data (especially the value of β in Eq. (4)) should allow for the determination of cooling rates based on isotopic ratios. The potential advantage of this method over the use of Ni profiles is that it does not rely on assumptions regarding kamacite nucleation or diffusion mechanisms. Comparison of these data with cooling rates determined from trace elements and Ni profiles may then help to better constrain the cooling history of asteroidal parent bodies.

5.3.2. The partial re-equilibration of pallasites

A second field of application of our results is the case of pallasites, which are classically interpreted as having formed at the core–mantle interface in differentiated asteroids [48]. They mainly consist of olivine and Fe-rich alloy in different modal proportions, and have been used to determine metal–silicate partition coefficients of highly siderophile elements. Several studies reported significant Fe isotope fractionation between metal and silicate fractions [4,9,62]. Although this fractionation varies from one sample to another, it is found that the metal fraction has on average an isotopic composition equal to or heavier than the silicate fraction. The range of metal–silicate fractionation documented so far varies from −0.06‰/a.m.u. to 0.1‰/a.m.u. [9,62]. These data suggest that some pallasites reached isotopic equilibrium between metal and olivine, but that others did not [9]. Our experimental data are consistent with this idea. If the lack of equilibrium were the result of a diffusion driven process such as that discussed above, then the observation in certain pallasites that the silicates are isotopically light relative to the metal leads to the somewhat surprising conclusion that during metal–silicate differentiation, Fe migrated from the metal to the silicate, rather than the other way around. In other words, the fractionation measured may indicate that the parent body underwent significant oxidation during its differentiation. It is worth noting that pallasites exhibit numerous disequilibrium features that may be consistent with this unexpected conclusion. The relatively high Fe-content of olivines coexisting with Fe-metal (e.g., the Brenham pallasite contains Fo_{88} olivine) may also be consistent with a late stage of oxidation. On the other hand, pallasitic olivines do not seem to show very clear radial gradients of decreasing Fe concentration [63,64], which may contradict the aforementioned hypothesis. In this case, several other explanations are possible. For example, even the "high" values of metal-olivine isotope fractionation may represent equilibrium values, being explained in terms of variable oxygen fugacities, differentiation temperatures and/or pressures at the time of pallasite formation.

Alternatively, it should be appreciated that the assemblage olivine+metal cannot be interpreted as a closed system because several geochemically important oxides found in planetary mantles are missing (e.g., Al_2O_3). It is thus still unclear if the isotopic fractionations measured in these natural rocks result from the segregation of metal from a silicate melt, or the fractionation of olivine from other silicate minerals during the crystallization of a hypothetical magma ocean. Recent data on inter-mineral fractionations in terrestrial mantle xenoliths [10] would not favor the latter hypothesis, but more experimental work is clearly needed to clarify this point. Finally, it is also possible that the isotopic fractionations measured in these rocks do not result from differentiation events, but from the mixing of metal and silicate of different origins. In this

latter case, pallasites should not be considered as core–mantle boundary material, but as breccias. If this is true, their use to constrain the properties and histories of planetesimal cores is questionable as already discussed by other authors [e.g., 65].

6. Conclusions

This experimental study demonstrates that significant fractionation of Fe isotopes may be produced by high-temperature, diffusion-controlled processes, in particular during segregation of Fe from a molten silicate to form a metallic alloy. During this segregation, the silicate reservoir becomes heavier and the alloy synthesized is isotopically lighter than the starting material. The parameter β which quantitatively relates the diffusion coefficients of different Fe isotopes to their difference in mass has been determined ($\beta \sim 0.27$). The value is very similar to that describing the diffusion-controlled fractionation of Ge when it alloys with Cu. This result indicates that diffusion-driven isotopic fractionation in metals might be described by a narrow range of values for β.

On the other hand, the characteristic time-scale for re-equilibration is short in our experiments. However, the time required to re-equilibrate both reservoirs depends on their respective volumes. Also, it is anticipated that temperature, pressure and the nature of the materials must affect the rate of re-equilibration since these parameters affect diffusion coefficients by several orders of magnitude.

As a consequence, isotopic fractionation of Fe may be a useful tool to test different models of core formation, such as those described by Rubie et al. [66]. If small droplets of metals equilibrated with a large volume of molten silicate, a complete re-equilibration of these isotopic reservoirs is expected. On the other hand, if metal–silicate equilibration occurred at the bottom of a magma ocean, between a thick layer of molten metal and a partially crystallized silicate mantle, fractionation of Fe isotopes between the core and the mantle may have been preserved.

In this respect, iron meteorites and pallasites are of particular interest. Obviously, the Fe isotopic signatures of pallasites and other igneous rocks are not straightforward but our study indicates that diffusion-driven fractionation is the most viable mechanism to fractionate iron isotopes significantly as a result of a change of redox state or some other intensive variable. As a consequence, iron isotopes constitute a very efficient probe to highlight non-equilibrium features of differentiated bodies.

Acknowledgements

The continuous help provided at the CRPG in clean lab by Céline Fournier and advice for platinum digestion by Luc Marin are much appreciated. We also thank Mary Horan and Tim Mock from DTM for the invaluable help provided in clean rooms and during analytical session on the Axiom, respectively. The help and comments provided by Maud Boyet are greatly appreciated. We thank Franck Poitrasson and an anonymous reviewer for their very careful reviews, which greatly improved the quality of this paper. This research was supported by funding from PICS no. 2051, and the French CNRS-INSU DyETI2005 program.

References

[1] B.L. Beard, C.M. Johnson, L. Cox, H. Sun, K.H. Nealson, C. Aguiliar, Iron isotope biosignatures, Science 285 (1999) 1889–1892.
[2] B.L. Beard, C.M. Johnson, High precision Fe isotope measurements of terrestrial and lunar materials, Geochim. Cosmochim. Acta 63 (1999) 1653–1660.
[3] X.K. Zhu, Y. Guo, R.K. O'Nions, E.D. Young, R.D. Ash, Isotopic homogeneity of Fe in the early solar nebula, Nature 412 (2001) 311–313.
[4] X.K. Zhu, Y. Guo, R.J.P. Williams, R.K. O'Nions, A. Matthews, N.S. Belshaw, G.W. Canters, E.C. de Waal, U. Weser, B.K. Burgess, B. Salvato, Mass fractionation processes of transition metal isotopes, Earth Planet. Sci. Lett. 200 (2002) 47–62.
[5] K. Kehm, E.H. Hauri, C.M. O'D. Alexander, R.W. Carlson, High precision Fe isotope measurements of meteoritic material by cold plasma ICP-MS, Geochim. Cosmochim. Acta 67 (2003) 2879–2891.
[6] N. Dauphas, M. van Zuilen, M. Wadhwa, A.M. Davis, B. Marty, P.E. Janney, Clues from Fe isotope variations on the origin of early Archean BIFs from Greenland, Science 306 (2004) 2077–2080.
[7] L.R. Croal, C.M. Johnson, B.L. Beard, D.K. Newman, Iron isotope fractionation by Fe(II)-oxidizing photoautotrophic bacteria, Geochim. Cosmochim. Acta 68 (2004) 1227–1242.
[8] F. Poitrasson, A.N. Halliday, D.-C. Lee, S. Levasseur, N. Teutsch, Iron isotope differences between Earth, Moon, Mars and Vesta as possible records of contrasted accretion mechanisms, Earth Planet. Sci. Lett. 223 (2004) 253–266.
[9] F. Poitrasson, S. Levasseur, N. Teutsch, Significance of Fe isotope mineral fractionation in pallasites and Fe meteorites for the core–mantle differentiation of terrestrial planets, Earth Planet. Sci. Lett. 234 (2005) 151–164.
[10] H.M. Williams, A.H. Peslier, C. McCammon, A.N. Halliday, S. Levasseur, N. Teutsch, J.-P. Burg, Systematic Fe isotope variations in mantle rocks and minerals: the effects of partial melting and oxygen fugacity, Earth Planet. Sci. Lett. 235 (2005) 435–452.
[11] J.L. Skulan, B.L. Beard, C.M. Johnson, Kinetic and equilibrium Fe isotope fractionation between aqueous Fe(III) and hematite, Geochim. Cosmochim. Acta 66 (2002) 2995–3015.
[12] S.A. Welch, B.L. Beard, C.M. Johnson, P.S. Braterman, Kinetic and equilibrium Fe isotope fractionation between aqueous Fe (II) and Fe(III), Geochim. Cosmochim. Acta 67 (2003) 4231–4250.

[13] R.A. Wiesli, B.L. Beard, C.M. Johnson, Experimental determination of Fe isotope fractionation between aqueous Fe(II) and "green rust" in abiotic systems, Chem. Geol. 211 (2004) 343–362.
[14] A. Kavner, F. Bonet, A. Shahar, J. Simon, E. Young, The isotopic effects of electron transfer: an explanation for the Fe isotope fractionation in nature, Geochim. Cosmochim. Acta 69 (2005) 2971–2979.
[15] V. Polyakov, Equilibrium fractionation of the Fe isotopes: estimation from Mössbauer spectroscopy data, Geochim. Cosmochim. Acta 61 (1997) 4213–4217.
[16] V. Polyakov, S.D. Mineev, The use of Mössbauer spectroscopy in stable isotope geochemistry, Geochim. Cosmochim. Acta 64 (2000) 849–865.
[17] E.A. Schauble, G.R. Rossman, H.P. Taylor Jr., Theoretical estimates of equilibrium Fe-isotope fractionations from vibrational spectroscopy, Geochim. Cosmochim. Acta 65 (2001) 2487–2497.
[18] N. Dauphas, P.E. Janney, R.A. Mendybaev, M. Wadhwa, F.M. Richter, A.M. Davis, M. van Zuilen, R. Hines, C.N. Foley, Chromatographic separation and multicollection-ICPMS analysis of Fe. Investigating mass-dependent and -independent isotope effects, Anal. Chem. 76 (2004) 5855–5863.
[19] A.M. Davis, R.N. Clayton, T.K. Mayeda, D.E. Brownlee, Large mass fractionation of iron isotopes in cosmic spherules collected from deep-sea sediments, Lunar Planet. Sci. XXII (1991) 281–282.
[20] G.F. Herzog, S. Xue, G.S. Hall, L.E. Nyquist, C.-Y. Shih, H. Wiesmann, D.E. Brownlee, Isotopic and elemental composition of iron, nickel, and chromium in type I deep-sea spherules: implications for origin and composition of the parent micrometeoroids, Geochim. Cosmochim. Acta 63 (1999) 1443–1457.
[21] S. Taylor, C.M. O'D. Alexander, J. Delaney, P. Ma, G.F. Herzog, C. Engrand, Isotopic fractionation of Fe, potassium, and oxygen in stony cosmic spherules: implications for heating histories and sources, Geochim. Cosmochim. Acta 69 (2005) 2647–2662.
[22] M. Roskosz, B. Luais, M.J. Toplis, Experimental determination of iron isotope fractionation during high temperature segregation of metal from silicate liquids: evaporation or diffusion? Lunar Planet. Sci. XXXVI (2005) 1959.
[23] B.A. Cohen, S. Levasseur, R.H. B. Zanda, A.N. Hewins, Isotopic mass fractionation of iron in chondrules, evaporation or reduction? Lunar Planet. Sci. XXXVI (2005) 1690.
[24] J. Schuessler, R. Schoenberg, H. Behrens, F. von Blanckenburg, Experimental calibration of the Fe isotope fractionation between pyrrhotite and silicate melt, Geochim. Cosmochim. Acta 69 (2005) A211.
[25] R. Hultgren, P.D. Desai, D.T. Hawkins, M. Gleider, K.K. Kelly, Selected values of the thermodynamic properties of binary alloys. ASM International, Metals Park, OH.
[26] K. Ito, G.C. Kennedy, Melting and phase relations in a natural peridotite to 40 kilobars, Am. J. Sci. 265 (1967) 519–538.
[27] R.B. Merill, P.J. Wyllie, Iron absorption by Pt capsules in high-pressure rock melting experiments, Am. Mineral. 58 (1973) 16–20.
[28] C.R. Stern, P.J. Wyllie, Effect of Fe absorption by noble-metal capsules on phase boundaries in rock-melting experiments at 30 kilobars, Am. Mineral. 60 (1975) 681–689.
[29] H.S. Yoder, C.E. Tilley, Origin of basalt magmas: experimental study of natural and synthetic rock systems, J. Petrol. 3 (1962) 342–532.
[30] T.L. Grove, Use of FePt alloys to eliminate the Fe loss problem in 1 atmosphere gas mixing experiments: Theoretical and practical considerations, Contrib. Mineral. Petrol. 78 (1981) 298–304.
[31] G. Gudmundsson, J.R. Holloway, Activity–composition relationships in the system Fe–Pt at 1300 and 1400 °C and at 1 atm and 20 kbar, Am. Mineral. 78 (1993) 178–186.
[32] J. Doleral, P. Povondra, Z. Sulcek, Decomposition Techniques in Inorganic Analysis, London Iliffe Books, New York American Elsevier Publishing Company Inc., 1968.
[33] C.N. Maréchal, P. Télouk, F. Albarède, Precise analysis of copper and zinc isotopic composition by plasma-source mass spectrometry, Chem. Geol. 156 (1999) 251–273.
[34] V. Magnien, D.R. Neuville, L. Cormier, B.O. Mysen, V. Briois, S. Belin, O. Pinet, P. Richet, Kinetics of iron oxidation in silicate melts: a preliminary XANES study, Chem. Geol. 213 (2004) 253–263.
[35] J. Crank, The Mathematics of Diffusion, Clarendon Press, 1975.
[36] H. Oikawa, Lattice Self-diffusion in Solid Iron; a Critical Review, Tech. Rep., vol. 46, Tohoku Univ, 1982, pp. 67–77.
[37] H.C. Watson, E.B. Watson, Siderophile trace element diffusion in Fe–Ni alloys, Phys. Earth Planet. Inter. 139 (2003) 65–75.
[38] K. Righter, A.J. Campbell, M. Humayun, Diffusion of trace elements in FeNi metal: applications to zoned metal grains in chondrites, Geochim. Cosmochim. Acta 69 (2005) 3145–3158.
[39] F.M. Richter, Y. Liang, A.M. Davis, Isotope fractionation by diffusion in molten oxides, Geochim. Cosmochim. Acta 63 (1999) 2853–2861.
[40] F.M. Richter, A.M. Davis, D.J. DePaolo, E.B. Watson, Isotope fractionation by chemical diffusion between molten basalt and rhyolite, Geochim. Cosmochim. Acta 67 (2003) 3905–3923.
[41] A. Tsuchiyama, K. Kawamura, T. Nakao, C. Uyeda, Isotopic effects on diffusion in MgO melt simulated by molecular dynamics (MD) method and implications for isotopic mass fractionation in magmatic systems, Geochim. Cosmochim. Acta 58 (1994) 3013–3021.
[42] T. Hehenkamp, A. Lodding, H. Odelius, V. Schlett, Isotope effect in the diffusion of the stable germanium isotopes in copper, Acta Metall. 27 (1979) 829–832.
[43] S.G. Nielsen, M. Rehkämper, A.N. Halliday, Large thallium isotopic variations in iron meteorites and evidence for lead-205 in the early solar system, Geochim. Cosmochim. Acta 70 (2006) 2643–2657.
[44] H.C. Urey, The thermodynamic properties of isotopic substances, J. Chem. Soc. (1947) 562–581.
[45] J. Grange, J.A. Shaw, The range of stability of the superlattice Pt_3Fe, Philos. Mag. 7 (1962) 207–212.
[46] Y. Mihsima, S. Ochiai, T. Suzuki, Lattice parameters of Ni(γ), $Ni_3Al(\gamma')$ and $Ni_3Ga(\gamma')$ solid solutions with additions of transition and B-subgroup elements, Acta Metall. 33 (1985) 1161–1169.
[47] E.R.D. Scott, J.T. Wasson, Classification and properties of Fe meteorites, Rev. Geophys. Space Phys. 13 (1975) 527–546.
[48] J.T. Wasson, Meteorites: Their Record of Early Solar System History, W.H. Freeman and Co., NY, 1985.
[49] J.A. Wood, Cooling rates and parent planets of several Fe meteorites, Icarus 3 (1964) 429–459.
[50] J.I. Goldstein, R.E. Ogilvie, The growth of the Widmanstätten pattern in metallic meteorites, Geochim. Cosmochim. Acta 29 (1965) 893–920.
[51] A.E. Moren, J.I. Goldstein, Cooling rates of group IVA Fe meteorites determined from a ternary Fe–Ni–P model, Earth Planet. Sci. Lett. 43 (1979) 182–196.
[52] C. Narayan, J.I. Goldstein, A major revision of Fe meteorite cooling rates—an experimental study of the growth of the

Widmanstätten pattern, Geochim. Cosmochim. Acta 49 (1985) 397–410.
[53] K.L. Rasmussen, The cooling rates of Fe meteorites—a new approach, Icarus 45 (1981) 564–576.
[54] K.L. Rasmussen, Cooling rates of IIIAB Fe meteorites, Icarus 80 (1989) 315–325.
[55] K.L. Rasmussen, H. Haack, F. Ulff-Moller, Metallographic cooling rates of group IIF Fe meteorites, Meteorit. Planet. Sci. 36 (2001) 883–896.
[56] C.W. Yang, D.B. Williams, J.I. Goldstein, A revision of the Fe–Ni phase diagram at low temperature, J. Phase Equilib. 17 (1996) 522–531.
[57] K. Braun-Dullaeus, K. Traxel, Copper, zinc, gallium and germanium distributions in taenite lamellae of Fe meteorites and their importance for cooling rate estimations, Planet. Space Sci. 43 (1995) 429–434.
[58] A. Meibom, C. Yang, M. Elfman, K.L. Rasmussen, Iron meteorites: Profiles of Ge, Ga, and Cu using m-PIXE, LPSC, vol. XXVII, 1996, p. 857, abstract volume.
[59] H.C. Watson, E.B. Watson, W.F. McDonough, R. Ash, Siderophile element profile measurements in Fe meteorites using laser ablation ICP-MS, LPSC, vol. XXXVI, 2005, p. 2141, abstract.
[60] E.R.D. Scott, H. Haack, T.J. McCoy, Core crystallization and silicate–metal mixing in the parent body of the IVA Fe and stony Fe meteorites, Geochim. Cosmochim. Acta 60 (1995) 1615–1631.
[61] H.C. Watson, E.B. Watson, Siderophile trace element diffusion in Fe–Ni alloys, Phys. Earth Planet. Inter. 139 (2003) 65–75.
[62] S. Weyer, A.D. Anbar, G.P. Brey, C. Münker, K. Mezger, A.B. Woodland, Iron isotopes fractionation during planetary differentiation, Earth Planet. Sci. Lett. 240 (2005) 251–264.
[63] P.R. Buseck, Pallasite meteorites—mineralogy, petrology and geochemistry, Geochim. Cosmochim. Acta 41 (1977) 711–740.
[64] M. Miyamoto, H. Takeda, Chemical zoning of olivine in Several Pallasites Suggestive of Faster Cooling, LPSC, vol. XXV, 1994, pp. 921–922.
[65] G.J. Taylor, Core formation in asteroids, J. Geophys. Res. 97 (1992) 14717–14726.
[66] D.C. Rubie, H.J. Melosh, J.E. Reid, C. Liebske, K. Righter, Mechanisms of metal–silicate equilibration in the terrestrial magma ocean, Earth Planet. Sci. Lett. 205 (2003) 239–255.